

## Research Article

**EVALUATION OF SOME NUCLEAR LEVEL DENSITY  
AND RADIATIVE STRENGTH FUNCTION MODELS BASED  
ON EXPERIMENTAL TWO-STEP GAMMA-CASCADE  
INTENSITIES OF  $^{51}\text{V}(n_{th}, 2\gamma)^{52}\text{V}$  REACTION***Nguyen Ngoc Anh<sup>1</sup>, Le Tan Phuc<sup>2</sup>, Nguyen Xuan Hai<sup>1</sup>, Nguyen Quang Hung<sup>2\*</sup>*<sup>1</sup>Dalat Nuclear Research Institute, Vietnam Atomic Energy Institute, Vietnam<sup>2</sup>Duy Tan University, Vietnam*\*Corresponding author: Nguyen Quang Hung – Email: [nguyenquanghung5@duytan.edu.vn](mailto:nguyenquanghung5@duytan.edu.vn)**Received: June 04, 2022; Revised: June 14, 2022; Accepted: June 23, 2022***ABSTRACT**

Some nuclear level density (NLD) and radiative strength function (RSF) models, including three phenomenological NLD and three phenomenological RSF models, and a microscopic model that simultaneously determines the NLD and RSF, have been evaluated based on the experimental two-step gamma-cascade intensities obtained from the  $^{51}\text{V}(n_{th}, 2\gamma)^{52}\text{V}$  experiment at the Dalat Nuclear Research Institute. Among the models evaluated, the exact pairing coupled with the independent-particle and phonon-damping models best explains the experimental data and is, thus, considered to be the most credible model to predict the NLD and RSF of  $^{52}\text{V}$ . To have a more comprehensive evaluation, forthcoming studies should assess a larger variety of models in particular, those that employ the mean-field Hartree-Fock-Bogoliubov approximation, as well as other  $(n_{th}, 2\gamma)$  experiments.

**Keywords:** nuclear level density; radiative strength function; two-step gamma-cascade intensities;  $^{51}\text{V}(n_{th}, 2\gamma)^{52}\text{V}$  reaction

**1. Introduction**

The evolution and synthesis of elements in the stellar environment and the origin of elemental abundance in our universe have been attractive topics in nuclear physics and astrophysics. The synthesis of present elements should be gone through several processes; one of them is the slow-neutron capture process (*s*-process).  $^{51}\text{V}(n, \gamma)^{52}\text{V}$  is one of the nuclear reactions in the *s*-process that produces heavier Vanadium and Chromium isotopes. Thus, its astrophysical reaction rate has been one of the important factors needed to be explored.

---

*Cite this article as:* Nguyen Ngoc Anh, Le Tan Phuc, Nguyen Xuan Hai, & Nguyen Quang Hung (2022). Evaluation of some nuclear level density and radiative strength function models based on experimental two-step gamma-cascade intensities of  $^{51}\text{V}(n_{th}, 2\gamma)^{52}\text{V}$  reaction. *Ho Chi Minh City University of Education Journal of Science*, 19(6), 897-907.

This reaction rate depends closely on the neutron energy and is characterized by the neutron-capture cross sections or the so-called  $(n, \gamma)$  cross section. As the electric and magnetic fields cannot accelerate neutron due to its neutral charge, the production of mono-energetic neutron beam has still been challenging. In fact, the  $^{51}\text{V}(n, \gamma)^{52}\text{V}$  cross-section data have been primarily measured for the neutron energy below 3 MeV (Exfor, 2022). Above this energy, most of the  $^{51}\text{V}(n, \gamma)^{52}\text{V}$  cross sections have been theoretically determined, for example, using the statistical Hauser-Feshbach model (Hauser & Feshbach, 1952). In the Hauser-Feshbach model, the nuclear level density (NLD) and radiative strength function (RSF) are among two key inputs that determine the reliability and accuracy of  $(n, \gamma)$  cross sections. However, the experimental measurements of these two quantities are not always easy. Hence, theoretical models of NLD and RSF are often used. One of the most advanced experimental methods to determine the NLD and RSF is the Oslo method. This method allows us to simultaneously extract NLD and RSF from the experimental gamma-ray spectra detected using light-ion induced reactions (Schiller et al., 2000). However, this method is only limited to the excitation or gamma energy region below the neutron binding energy ( $B_n \sim 8$  MeV). At the same time, the calculations of  $(n, \gamma)$  cross section require the excitation and gamma energies up to about 150 MeV. In this case, the Oslo data of NLD and RSF can be used as a testing ground for various NLD and RSF models. Unfortunately, no experimental measurement of NLD and RSF of  $^{52}\text{V}$  nucleus has been done. Thus, it is still difficult to test the predictive power of NLD and RSF models for this nucleus.

The two-step gamma-cascade (TSC) intensities obtained from the  $(n_{th}, 2\gamma)$  reactions can be directly calculated from the NLD and RSF (Boneva et al., 1995). Therefore, the accuracy of theoretical NLD and RSF models can be evaluated by comparing the theoretical TSC spectra (obtained by using theoretical NLD and RSF) with those determined from the  $(n_{th}, 2\gamma)$  reaction, especially for the case of  $^{52}\text{V}$  nucleus, whose NLD and RSF data are unavailable. In the present study, the TSC intensity distribution of  $^{52}\text{V}$  was measured by using the  $^{51}\text{V}(n_{th}, 2\gamma)^{52}\text{V}$  reaction at Dalat nuclear research institute (DNRI). The obtained distribution was then used to evaluate different phenomenological and microscopic NLD and RSF models.

## 2. Methods

### 2.1. Experimental determination of two-step gamma-cascade intensities of $^{52}\text{V}$

To determine the experimental TSC intensities of  $^{52}\text{V}$ , we measured the coincident gamma rays emitted from the  $^{51}\text{V}(n_{th}, 2\gamma)^{52}\text{V}$  reaction using the gamma-gamma coincident spectrometer (Pham et al., 2011) and thermal neutron source from DNRI. The experimental configuration and details, except the target and measuring time, are the same as those presented in our recent publications (Nguyen et al., 2017; Nguyen et al., 2019), so we do not repeat them here. In the present experiment, a natural Vanadium target of 1.5 g containing about 99.75% of  $^{51}\text{V}$  was measured in about 400 hours. The obtained two-dimensional (2D)

gamma coincident spectrum is presented in Figure 1. By selecting all the gamma coincident events having total energy of  $7311 \pm 8$  keV (equivalent to the neutron binding energy  $B_n$  and the peak resolution of gamma-gamma coincident spectrometer) and projecting the 2D spectrum onto the x and y axes, we obtained the relative TSC intensities corresponding to the gamma transition from the compound state of  $^{52}\text{V}$  to its ground state. This TSC intensity distribution was then corrected following a correction due to the difference in the efficiencies of two HPGe detectors, prior to being normalized to the absolute intensities based on the intensities of a (6517.7 keV, 793.5 keV) gamma transition (0.03479/captures) (Lumengalo et al., 2014). Details on the determination of TSC intensities can be found in previous reports (Boneva et al., 1995; Nguyen, 2018).

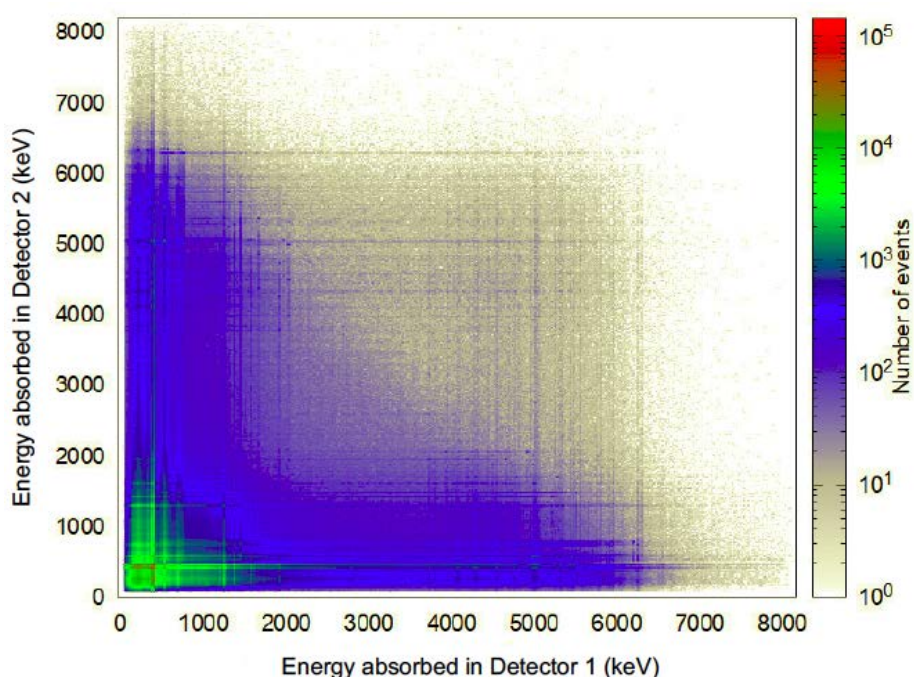


**Figure 1.** Two-dimensional gamma-gamma coincident spectrum of  $^{52}\text{V}$  obtained from the  $^{51}\text{V}(n_{th}, 2\gamma)^{52}\text{V}$  reaction

## 2.2. NLD and RSF models

Table 1 lists the NLD and RSF models used in the present work. Three phenomenological NLD (CTM, BSFG, and BSFGED) and three phenomenological RSF (SLO, MLO, and EGLO) models were used. In addition, a recent microscopic model of both NLD and RSF (EP+IPM & EP+PDM) was employed. The formalism and related references of these models are also presented in Table 1.

As for the microscopic model, the NLD was calculated from the EP+IPM method based on a canonical-ensemble partition function  $Z_{\text{EP+IPM}}$  (Nguyen & Nguyen, 2009). This partition function was constructed by taking into account all the solutions of the exact pairing (EP) problem plus the finite-temperature independent-particle model (IPM) (Nguyen et al., 2017). All the nuclear thermodynamic quantities, such as free energy ( $F$ ), entropy ( $S$ ),

average energy ( $E$ ), excitation energy ( $E^*$ ), and heat capacity ( $C$ ), can be easily calculated, namely  $F = -T \ln Z$ ,  $S = -\partial F / \partial T$ ,  $E = F + TS$ ,  $E^*(T) = E(T) - E(0)$ , and  $C = \partial E / \partial T$ . These quantities were then used to determine the total NLD

$$\rho_{tot}(E^*) = \rho_{int}(E^*) \times k_{vib} \times k_{rot}, \quad (2.1)$$

where  $\rho_{int}(E^*) = \frac{\omega(E^*)}{\sigma_{\parallel} \sqrt{2\pi}}$  is the intrinsic level density;  $\omega(E^*) = \frac{e^S}{T \sqrt{2\pi C}}$  is the total state density; and  $\sigma_{\parallel}$  is the parallel spin cut-off factor. In this work, all the parameters, such as the parallel spin cut-off ( $\sigma_{\parallel}$ ), perpendicular spin cut-off ( $\sigma_{\perp}$ ), vibrational enhancement  $k_{vib}$ , and rotational enhancement ( $k_{rot}$ ) factors, were calculated following our latest publication (Nguyen et al., 2022), namely

$$\sigma_{\perp}^2 = \frac{1}{2} \sum_k m_k^2 \operatorname{sech}^2 \frac{1}{2} (E_k/T), \quad \sigma_{\parallel} = \sigma_{\perp} \sqrt{(3 - 2\beta_2)/(3 + \beta_2)}, \quad (2.2)$$

$$k_{vib} = \exp \left[ \delta S - \frac{\delta U}{T} \right], \quad k_{rot} = \frac{\sigma_{\perp}^2 - 1}{1 + e^{(E^* - U_C)/D_C}} + 1, \quad (2.3)$$

where  $m_k$  is the spin projection of a single-particle state  $|k\rangle$  in the deformed basis;  $E_k = \sqrt{(\epsilon_k - \lambda)^2 + \Delta^2}$  is the quasiparticle energy;  $\beta_2$  is the quadrupole deformation parameter;  $\delta S = \sum_i (2\lambda_i + 1) [(1 + n_i) \ln(1 + n_i) - n_i \ln n_i]$  is the variation of entropy;  $\delta U = \sum_i (2\lambda_i + 1) \omega_i n_i$  is the variation of excitation energy;  $U_C = 1400 \beta_2^2 A^{-2/3}$  and  $D_C = 120 \beta_2^2 A^{1/3}$  ( $A$  is the mass number). The quantities  $\omega_i$ ,  $\lambda_i$ , and  $n_i$  are vibrational phonon energy, multipolarity, and temperature-dependent occupation number, respectively. The occupation number  $n_i$  can be expressed via

$$n_i = \frac{\exp(-\gamma_i/2\omega_i)}{\exp\left(\frac{\omega_i}{T}\right) - 1}, \quad (2.4)$$

where  $\gamma_i = 0,0075 A^{1/2} (\omega_i^2 + 4\pi^2 T^2)$  is the spreading width of vibrational motion. For the vibrational phonon energy  $\omega_i$ , two strongest modes corresponding to the octupole ( $\lambda = 2$ ) and hexadecapole ( $\lambda = 3$ ) vibrations are often used (Hilaire & Goriely, 2006)

$$\omega_2 = \frac{65 A^{-5/6}}{1 + 0,05 E_{Shell}}, \quad \omega_3 = \frac{100 A^{-5/6}}{1 + 0,05 E_{Shell}}, \quad (2.5)$$

where  $E_{Shell}$  is the shell-correction energy determined from the difference between the theoretical and experimental masses (Capote et al., 2009). Practically, the EP+IPM calculation for the NLD used the following parameters: the pairing strengths for the neutron ( $G_N$ ) and proton ( $G_Z$ ) (being adjusted so that the calculated pairing gaps at  $T = 0$  fit the experimentally extracted ones); quadrupole deformation parameter  $\beta_2$  (being selected from the RIPL database (Capote et al., 2009)), and shell-correction energy  $E_{Shell}$ . The values of these parameters for  $^{52}\text{V}$  nucleus are given in Table 2.

**Table 1.** List of the NLD and RSF models used in the present work for  $^{52}\text{V}$  nucleus

Model	Abbreviation	Model type	Reference
Constant temperature model	CTM	NLD	Von Egidy & Bucurescu, 2005 and references therein
Back-shifted Fermi gas	BSFG	NLD	Von Egidy & Bucurescu, 2005 and references therein
Back-shifted Fermi gas with energy dependence	BSFGED	NLD	Von Egidy & Bucurescu, 2005 and references therein
Standard Lorentzian	SLO	RSF	Belgya et al., 2006 and references therein
Modified Lorentzian	MLO	RSF	Belgya et al., 2006 and references therein
Enhanced Generalized Lorentzian	EGLO	RSF	Belgya et al., 2006 and references therein
Exact Pairing + Independent-Particle Model (EP+IPM) & Exact Pairing + Phonon-Damping Model (EP+PDM)	EP+IPM & EP+PDM	NLD & RSF	Nguyen, et al., 2017

As for the RSF, it was calculated within the EP+PDM by combining the EP with the phonon-damping model (PDM) (Nguyen & Arima, 1998). Within the EP+PDM, the RSF for a given multipole electromagnetic transition XL ( $X = E$  for electric;  $X = M$  for magnetic;  $L = 1, 2, 3$ , etc for monopole, dipole, octupole, etc) is calculated as (Nguyen et al., 2017)

$$f_{XL}(E_\gamma, T) = \left( \frac{1}{(2L + 1)\pi^2 \hbar^2 c^2} \right) \frac{\pi \sigma_{XL} \Gamma_{XL}(E_\gamma, T) S_{XL}(E_\gamma, T)}{E_\gamma}, \quad (2.6)$$

where  $1/(\pi^2 \hbar^2 c^2) = 26 \times 10^{-8}$ ;  $S_{XL}(E_\gamma, T) = \frac{\gamma_{XL}(E_\gamma, T)}{(E_\gamma - E_{XL})^2 + \gamma_{XL}^2(E_\gamma, T)}$  is the PDM strength function;  $\sigma_{XL}$  is the cross section that is independent of  $E_\gamma$  và  $T$ ; and  $\Gamma_{XL}(E_\gamma, T) = 2\gamma_{XL}(E_\gamma, T)$  is the spreading width. The total RSF is the sum of its components, that is,  $f_{tot} = f_{E1} + f_{M1} + f_{E2}$ . Each RSF component is characterized by the resonance energy  $E_{XL}$ , resonance width  $\Gamma_{XL}$ , and cross section  $\sigma_{XL}$ . The values of these parameters are often selected from the corresponding experimental data or the recommended global parameters by Dietrich-Berman or Steinwedel-Jensen (Belgya et al., 2006). For light and medium nuclei, there should be an additional RSF component called the upbending RSF ( $f_{ub}$ ) in the energy region below  $\sim 2$  MeV (Larsen & Goriely, 2010)<sup>1</sup>, whereas for heavy nuclei, there appears a pygmy RSF ( $f_{py}$ ) caused by the pygmy dipole resonance (PDR) in the energy region of 2-4 MeV (Nyhus et al., 2010).

<sup>1</sup> Upbending is an effect that the RSF is relatively large at  $E_\gamma \sim 0$  MeV, decreases with increasing  $E_\gamma$  from 1-2 MeV, and increases at  $E_\gamma > 1-2$  MeV.

In this study, the total RSF of  $^{52}\text{V}$  was calculated within the EP+PDM as  $f_{tot} = f_{E1} + f_{M1} + f_{ub}$  (the E2 RSF was neglected due to its tiny contribution). In addition, as  $^{52}\text{V}$  is a deformed nucleus with  $\beta_2 = 0.053$  MeV (oblate deformation), its E1 resonance is, in general, split into two smaller resonances with energies  $E_1^I$  and  $E_1^{II}$  and widths  $\Gamma_1^I$  and  $\Gamma_1^{II}$ . Thus, there are two corresponding RSFs  $f_{E_1^I}$  and  $f_{E_1^{II}}$ . All the parameters of  $f_{E_1^I}$ ,  $f_{E_1^{II}}$ ,  $f_{M1}$ , and  $f_{ub}$  are listed in Table 2.

**Table 2.** Values of all parameters used in the EP+IPM & EP+PDM calculations for the total NLD and the E1, M1, and upbending RSFs of  $^{52}\text{V}$

Parameter	Value
Energy of the first E1 resonance, $E_1^I$	17.9 MeV
Cross section of the first E1 resonance, $\sigma_{E_1^I}^I$	53.3 mb
Width of the first E1 resonance, $\Gamma_{E_1^I}^I$	3.6 MeV
Energy of the second E1 resonance, $E_1^{II}$	21.0 MeV
Cross section of the second E1 resonance, $\sigma_{E_1^{II}}^{II}$	40.7 mb
Width of the second E1 resonance, $\Gamma_{E_1^{II}}^{II}$	7.2 MeV
Energy of the M1 resonance, $E_{M1}$	11.1 MeV
Cross section of the M1 resonance, $\sigma_{M1}$	4.0 mb
Width of the M1 resonance, $\Gamma_{M1}$	0.5 MeV
Energy of the upbending resonance, $E_{ub}$	1.0 MeV
Cross section of the upbending resonance, $\sigma_{ub}$	0.2 mb
Width of the upbending resonance, $\Gamma_{ub}$	1.2 MeV
Ground-state quadrupole deformation parameter, $\beta_2$	0.053 MeV
Shell-correction energy, $E_{shell}$	0.183 MeV
Pairing strength for the neutrons, $G_N$	0.720 MeV
Pairing strength for the protons, $G_Z$	0.660 MeV

It is known that the phenomenological models listed in Table 1 cannot simultaneously describe the NLD and RSF. We, therefore, used different combinations of them to calculate the TSC intensity distribution. To evaluate these models, we have employed the conventional least-square method with

$$\chi^2 = \sum_{i=1}^n \left( \frac{I_{\gamma\gamma}^{exp} - I_{\gamma\gamma}^{theor}}{\Delta I_{\gamma\gamma}^{exp}} \right)_i^2, \tag{1}$$

where  $n$  is the number of experimental data points;  $I_{\gamma\gamma}^{exp}$  and  $I_{\gamma\gamma}^{theor}$  are, respectively, the experimental and theoretical TSC intensities; and  $\Delta I_{\gamma\gamma}^{exp}$  is the experimental error of  $I_{\gamma\gamma}^{exp}$ . The best NLD and/or RSF models should result in the smallest  $\chi^2$  value.

3. Results and discussion

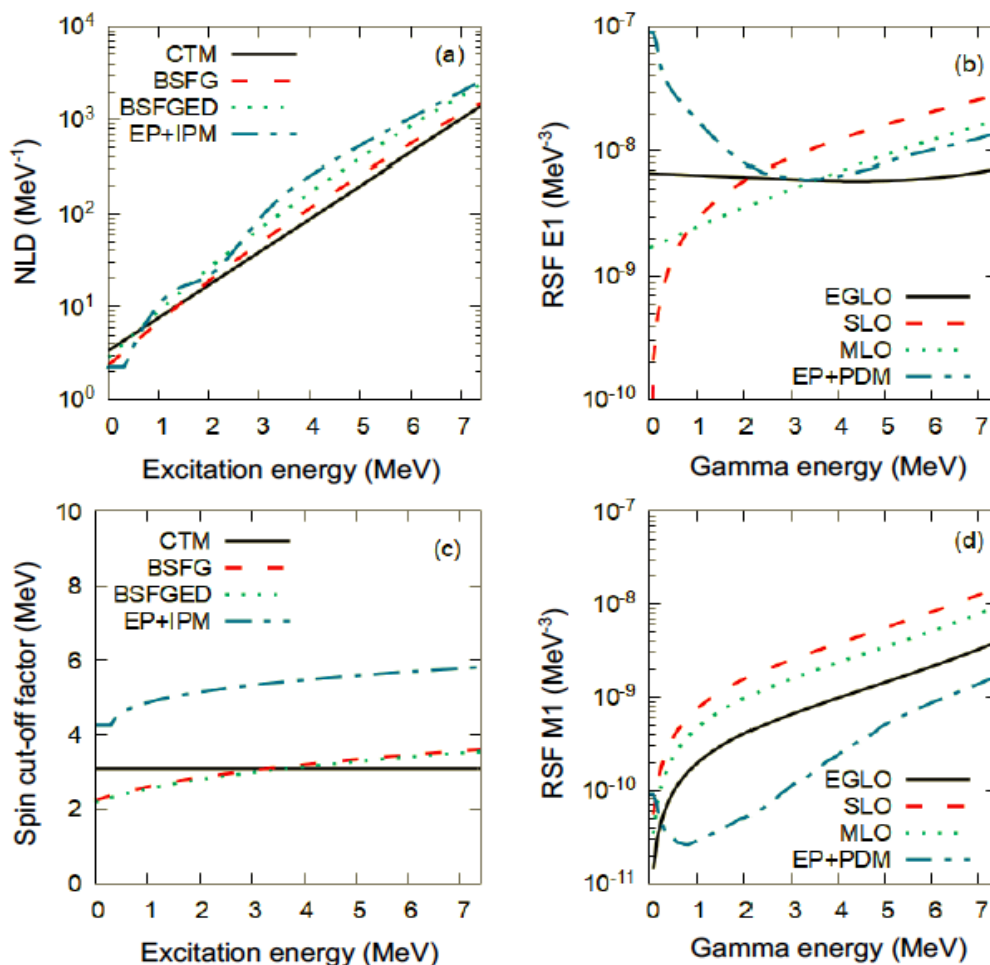


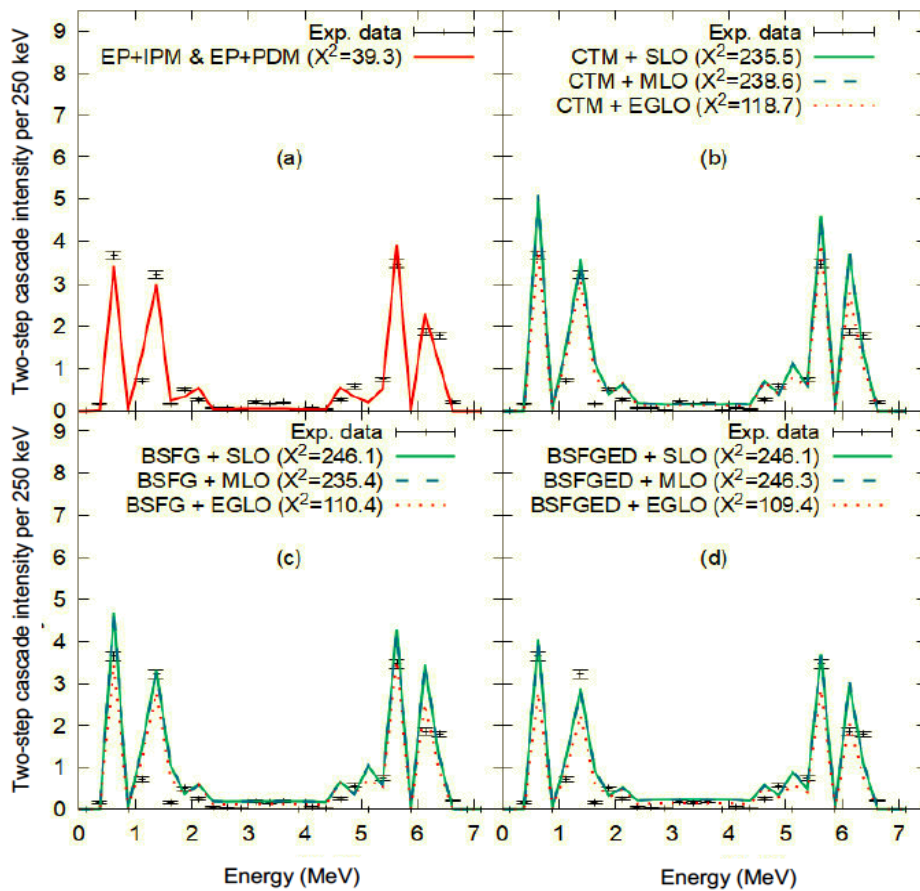
Figure 2. NLD (a), E1 RSF (b), M1 RSF (d), and spin cut-off factor (c) obtained by using different NLD and RSF models of <sup>52</sup>V

Figure 2 shows the NLD and RSFs (E1 and M1) obtained using different models in Table 1. It is seen in Figure 2a that, in the low-energy region, the difference between the NLDs obtained within different NLD models is not too large. In the high-energy region, the EP+IPM and BSFGED models predict the NLDs relatively higher than the CTM and BSFG predictions. In Figure 2c, the spin cut-off factor obtained within different NLD models, except the CTM, increases with increasing the energy, whereas the EP+IPM predicts the largest spin cut-off.

The RSFs for E1 and M1 resonances are plotted in Figures 2b and 2d, respectively. The E1 RSF predicted by the EP+PDM is highest at  $E_\gamma \sim 0$  MeV and gradually decreases with increasing  $E_\gamma$  up to about 3 MeV, due to the upbending effect. In contrast, the E1 RSF obtained by using the SLO is unphysically small at  $E_\gamma \sim 0$  MeV and strongly increases with increasing  $E_\gamma$  below about 2 MeV. This is a well-known shortcoming of the SLO model. The MLO model has solved this SLO problem, as seen in Figure 2b. The E1 EGLO is varied

very slightly at  $E_\gamma < 7.3$  MeV. For the M1 resonance, three phenomenological models predict similar behavior of RSFs. These M1 RSFs are only different in their magnitudes because they are all normalized based on their E1 RSFs (see e.g., Section 7.7 of (Belgya et al., 2006)), whereas the M1 RSF obtained within the EP+PDM exhibits a different shape and magnitude (Figure 2d).

In Figure 3, the theoretical TSC intensities are compared with the experimental data. Considering the pairs that used the same NLD model, the intensities obtained using the SLO and MLO RSFs are not much different, while those obtained using the EGLO are significantly different. It can be easily seen also in Figure 3 that the EP+IPM & EP+PDM best describe the experimental TSC intensities as it offers the smallest  $\chi^2$  value (39.3). Figure 4 shows that the combination of phenomenological NLD models with two RSF models of SLO and MLO results in relatively large  $\chi^2$  values ( $\chi^2 > 230$ ). Among the pairs of phenomenological NLD and RSF models, the BSFGED + EGLO offers the best result ( $\chi^2 = 109.4$ ). This result is understandable since these two models (BSFGED and EGLO) are more complex and contain more physical information than the remaining phenomenological models.



**Figure 3.** Comparison of theoretical and experimental TSC intensities of  $^{52}\text{V}$ . The intensities were normalized to 100 capture events

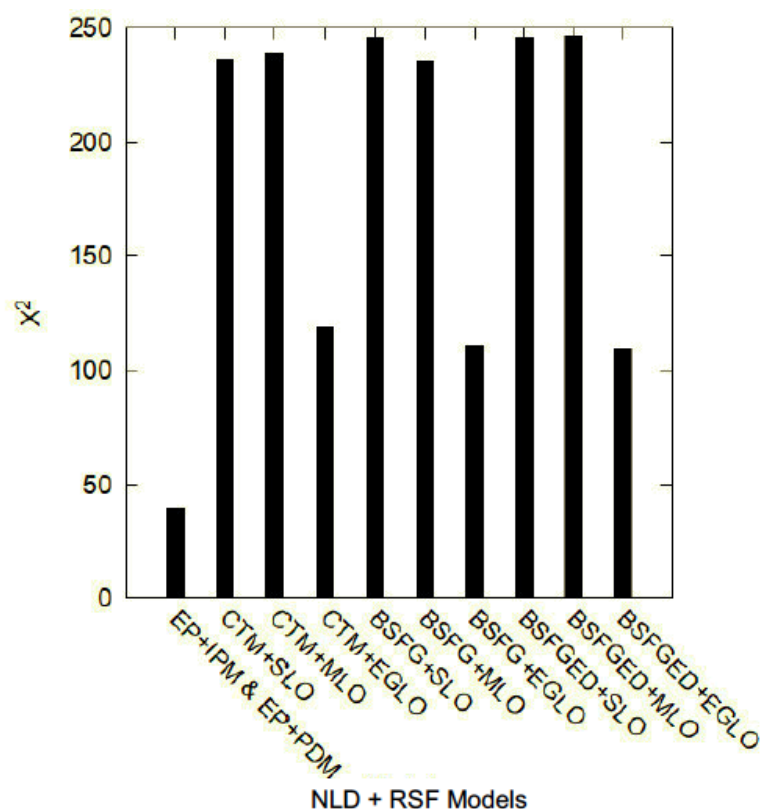


**Figure 4.** Comparison of  $\chi^2$  values obtained using different combinations of NLD and RSF models of  $^{52}\text{V}$

#### 4. Conclusions

In the present work, some phenomenological and microscopic models of NLD and RSF of  $^{52}\text{V}$  nucleus have been evaluated based on the TSC intensity distribution obtained from the  $^{51}\text{V}(n_{\text{th}}, 2\gamma)^{52}\text{V}$  reaction at Dalat Nuclear Research Institute. Results obtained show that the microscopic EP+IPM & EP+PDM model exhibits the highest reliability as it best describes the experimental data with the smallest  $\chi^2$  value. Among the phenomenological models, the BSFGED model for the NLD combined with the EGLO model for the RSF offers the best fit to the measured data. To have a broader view, more microscopic NLD and RSF models will be used in our subsequent studies, particularly those built on top of the Hartree-Fock-Bogoliubov (HFB) mean field. In addition, other  $(n_{\text{th}}, 2\gamma)$  reactions are also required, whereas the statistics of the  $^{51}\text{V}(n_{\text{th}}, 2\gamma)^{52}\text{V}$  reactions are also needed to improve so that the evaluation can be performed based on the TSC intensity distribution within a narrower energy bin (about 100 keV instead of 250 keV as in this study).

- ❖ **Conflict of Interest:** Authors have no conflict of interest to declare.
- ❖ **Acknowledgements.** This work was funded by the Ministry of Science and Technology under the Program of Development in Physics, Grant number ĐTĐLCN.02/19.

## REFERENCES

- Belgya, T., Bersillon, O., Capote, R., Fukahori, T., Zhitang, G., Goriely, S., Herman, M. Ignatyuk, A.V., Kailas, S., Koning, A., Obložinsky, P., Plujko, V., & Young, P. (2006). Handbook for calculations of nuclear reaction data. *IAEA-TECDOC-1506*.
- Boneva, S. T., Khitrov, V. A., Sukhovoij, A. M., & Vojnov, A. V. (1995). Excitation study of high-lying states of differently shaped heavy nuclei by the method of two-step cascades. *Nuclear Physics A*, 589, 293.
- Capote, R., Hermanet, M., Obložinský, P., Young, P. G., Goriely S.,... Talou, P. (2009). RIPL-reference input parameter library for calculation of nuclear reactions and nuclear data evaluations. *Nuclear Data Sheets*, 110(12), 3107-3214.
- EXFOR Database. (2022). Retrieved from <https://www-nds.iaea.org/exfor/>
- Hilaire, S., & Goriely, S. (2006). Global microscopic nuclear level densities within the HFB plus combinatorial method for practical applications. *Nuclear Physics A*, 779, 63-81.
- Hauser, W., & Feshbach, H. (1952). The Inelastic Scattering of Neutrons. *Physical Review*, 87, 366.
- Nguyen, D. D., & Arima, A. (1998). Quantal and Thermal Dampings of Giant Dipole Resonances in  $^{90}\text{Zr}$ ,  $^{120}\text{Sn}$ , and  $^{208}\text{Pb}$ . *Physical Review Letters*, 80, 4145.
- Nguyen, N. A., Nguyen, X. H., Pham, D. K., Nguyen, Q. H., & Ho, H. T. (2017). Updated level scheme of  $^{172}\text{Yb}$  from  $^{171}\text{Yb}(n_{th}, \gamma)$  reaction studied via gamma-gamma coincidence spectrometer. *Nuclear Physics A*, 964, 55.
- Nguyen, N. A. (2018). *Experimental study on level structure of excited  $^{172}\text{Yb}$  and  $^{153}\text{Sm}$  nuclei using neutron beam from Dalat nuclear research reactor*. PhD thesis, Vietnam Atomic Energy Institute.
- Nguyen, N. A., Nguyen, Q. H., Nguyen, X. H., Pham, D. K., Sukhovoij, A. M., Mitsyna, L. V., Ho, H. T., & Le, H. K. (2019). Level scheme of  $^{153}\text{Sm}$  obtained from the  $^{152}\text{Sm}(n_{th}, \gamma)$  reaction using a gamma-gamma coincidence spectrometer. *Physical Review C*, 100(2), 024324.
- Nguyen, N. L., Cristallo, S. Vescovi., Le, T. P., & Nguyen, Q. H. (2022). Maxwellian-averaged cross-section of  $^{181}\text{Ta}(n, \gamma)$  reaction and its astrophysical implications. *Nuclear Physics A*, 1023, 122450.
- Nguyen, Q. H., & Nguyen, D. D. (2009). Exact and approximate ensemble treatments of thermal pairing in a multilevel model. *Physical Review C*, 79, 054328.
- Nguyen, Q. H., Nguyen, D. D., & Le, T. Q. H. (2017). Simultaneous Microscopic Description of Nuclear Level Density and Radiative Strength Function. *Physical Review Letters*, 118, 022502.
- Nyhus, H. T., Siem, S., Guttormsen, M., Larsen, A. C., Burger, A., Syed, N. U. H., Tveten, G. M., & Voinov, A. (2010). Radiative strength functions in  $^{163,164}\text{Dy}$ . *Physical Review C*, 81, 024325.

- Larsen, A. C., & Goriely, S. (2010). Impact of a low-energy enhancement in the  $\gamma$ -ray strength function on the neutron-capture cross section. *Physical Review C*, 82, 014318.
- Lumengano, M., Pham, D. K., Nguyen, X. H., Nguyen, N. A., & Sukovoj, A. M. (2014). *Parameters of Cascade Gamma-Decay  $^{52}\text{V}$  and  $^{64}\text{Cu}$  Compound-States*. Proceeding of International Seminar on Interaction of Neutrons with Nuclei, Dubna, Russia.
- Pham, D. K., Nguyen, X. H., Vuong, H. T., & Nguyen, N. D. (2011). Gamma-gamma coincidence spectrometer setup for neutron activation analysis and nuclear structure studies. *Nuclear Instruments and Methods in Physics Research, Section A: Accelerators, Spectrometers, Detectors and Associated Equipment*, 634, 47.
- Schiller, A., Bergholt, L., Guttormsen, M., Melby, E., Rekstad, J., & Siem, S. (2000). Extraction of level density and  $\gamma$  strength function from primary  $\gamma$  spectra. *Nuclear Instruments and Methods in Physics Research Section A: Accelerators, Spectrometers, Detectors and Associated Equipment*, 447, 498.
- Von Egidy, T., & Bucurescu, D. (2005). Systematics of nuclear level density parameters. *Physical Review C*, 72, 044311.

**ĐÁNH GIÁ MỘT SỐ MÔ HÌNH MẬT ĐỘ MỨC VÀ HÀM LỰC BỨC XẠ  
DỰA TRÊN PHÂN BỐ CƯỜNG ĐỘ PHÂN RÃ GAMMA NỔI TẦNG THỰC NGHIỆM  
CỦA PHẢN ỨNG  $^{51}\text{V}(n_{th}, 2\gamma)^{52}\text{V}$**

**Nguyễn Ngọc Anh<sup>1</sup>, Lê Tấn Phúc<sup>2</sup>, Nguyễn Xuân Hải<sup>1</sup>, Nguyễn Quang Hưng<sup>2\*</sup>**

<sup>1</sup>*Viện Nghiên cứu Hạt nhân, Viện Năng lượng Nguyên tử Việt Nam, Việt Nam*

<sup>2</sup>*Trường Đại học Duy Tân, Việt Nam*

*\*Tác giả liên hệ: Nguyễn Quang Hưng – Email: nguyenguanghung5@duytan.edu.vn*

*Ngày nhận bài: 04-6-2022; ngày nhận bài sửa: 14-6-2022; ngày duyệt đăng: 23-6-2022*

**TÓM TẮT**

Một số mô hình mật độ mức (MĐM) và hàm lực bức xạ (HLBX), trong đó bao gồm 3 mô hình MĐM, 3 mô hình HLBX hiện tượng luận, và 1 mô hình vi mô xác định đồng thời MĐM và HLBX, đã được đánh giá dựa trên phân bố cường độ phân rã gamma nổi tầng thực nghiệm thu được từ thí nghiệm  $^{51}\text{V}(n_{th}, 2\gamma)^{52}\text{V}$  tại Viện Nghiên cứu Hạt nhân Đà Lạt. Trong số các mô hình được khảo sát, mô hình vi mô kết hợp lời giải chính xác bài toán kết cặp với mô hình đơn hạt độc lập và mô hình suy giảm phonon cho phép mô tả tốt nhất số liệu thực nghiệm và do đó có thể coi là mô hình tin cậy nhất để mô tả MĐM và HLBX của hạt nhân  $^{52}\text{V}$ . Để có thể đánh giá một cách tổng quát hơn, các nghiên cứu tiếp theo sẽ mở rộng số lượng các mô hình tham gia đánh giá, đặc biệt là các mô hình vi mô sử dụng phương pháp trường thế trung bình Hartree-Fock-Bogoliubov, cũng như với các phân ứng  $(n_{th}, 2\gamma)$  khác nhau.

**Từ khóa:** cường độ phân rã gamma nổi tầng bậc hai; hàm lực bức xạ; mật độ mức; phản ứng  $^{51}\text{V}(n_{th}, 2\gamma)^{52}\text{V}$